NN interaction from bag-model quark interchange

Bakker, B.L.G.; Bozoian, M.; Maslow, J.N.; Weber, H.J.

published in
Physical Review C
1982

DOI (link to publisher)
10.1103/PhysRevC.25.1134

document version
Publisher's PDF, also known as Version of record

PHYSICAL REVIEW C VOLUME 25, NUMBER 3 MARCH 1982

NN interaction from bag-model quark interchange

B. L. G. Bakker
Natuurkundig Laboratorium, Vrije Universiteit, Amsterdam, The Netherlands

M. Bozoian, J. N. Maslow, and H. J. Weber
Department of Physics, University of Virginia, Charlottesville, Virginia 22901
(Received 16 October 1981)

A partial-wave helicity-state analysis of elastic nucleon-nuclon scattering is carried out in momentum space. Its basis is a one- and two-boson exchange amplitude from a bag-model quark interchange mechanism. The resulting phase shifts and bound-state parameters of the deuteron are compared with other meson theoretic potentials and data up to laboratory energies of ~ 350 MeV.

[NUCLEAR REACTIONS *NN* elastic scattering, $E_{\text{lab}} \leq 350$ MeV. Coupling constants, form factors of renormalized OBE calculated from bag-model quark interchange. Phase shifts, deuteron parameters calculated from covariant partial-wave analysis.]

I. INTRODUCTION

Elastic nucleon-nucleon scattering at low energies below the pion production threshold and at medium to long internucleon distances is well described by a potential model derived from one-boson exchange (OBE) and two-pion exchange (TPE).[1] The TPE of the Paris potential[2] is related to πN phase shift data by means of t-channel dispersion relations. The Bonn potential[3] generates some TPE from s-channel $NN \rightarrow \Delta N$ and $NN \rightarrow \Delta\Delta$ transition potentials. Its OBE requires additional phenomenological scalar-isoscalar meson (σ_0) exchange. In both approaches nucleons are treated as point particles and their finite size is then taken into account by means of form factors. The OBE coupling constants and form factors are not calculated but either fitted to *NN* phase shifts or related to other data.

In the past few years, an SU(3) color gauge theory (quantum chromodynamics, QCD, Ref. 4) has become a candidate for a strong interaction theory. It is widely believed that QCD would have to provide an explanation of the meson exchange mechanism and the little understood *NN* amplitude at short range. The success of the OBE + TPE model is somewhat surprising because nucleons are now known to be extended particles, consisting predominantly of three valence quarks, with a mean square radius of ~ 0.85 fm so that they barely fit into nuclei without overlapping. Eventually QCD must also reconcile at long range the chiral aspects of the pion as a Nambu-Goldstone mode with its SU(6) quark-antiquark bound-state nature that it shares with the heavier mesons.

However, asymptotic freedom[5] holds in QCD, and this makes renormalized perturbation theory applicable, but only at high four-momentum transfer q. At low q when the effective quark-gluon coupling $\alpha_c = g^2/4\pi$ is large, color confinement is expected to govern strong interaction processes. It is not known in detail how this comes about. Therefore, phenomenological models have been developed which impose quark and gluon confinement by means of a local potential, which is either taken as a potential linear in the radial distance r of a quark from the hadron's center of mass, a harmonic oscillator, or an infinite square well in the MIT bag model.[6] Here we adopt the latter as a convenient and successful description of hadron spectroscopy which realizes color confinement in terms of boundary conditions.

In the past few years, several attempts[7] were made to obtain also the *NN* interaction from an effective quark-quark potential acting between the six valence quarks of two more or less overlapping nucleon bags. The results are rather model dependent

and inconclusive. There is now increasing evidence that the strong interactions at low energy and long range cannot be obtained from such a "quark-molecular" approach.[8] In fact, when α_c becomes sufficiently large, i.e., $\alpha_c \geq 0.37$, gluon pairing[9] appears to occur in the QCD vacuum and, for $\alpha_c \geq \frac{9}{8}$, it has been suggested that also quark-antiquark condensation[10] sets in. These condensates imply nonlocal effective quark interactions.[11]

In this framework it has been suggested[12] that the meson (i.e., quark-antiquark) exchange of the OBEP translates into a nonlocal, nonperturbative quark interchange mechanism between hadrons. This mechanism (cf. Figs. 1 and 2) has been shown[12,13] to produce interactions of the same algebraic structure as the OBE + TBE + $\cdots$ expansion. Moreover, the coupling constants and form factors of hadronic vertices that are calculated are in agreement with the measured values within the uncertainties of the MIT bag model. The mesonic vertex invariants are generated from the basic quark-gluon vector coupling $ig\gamma_\mu \frac{1}{2}\lambda^a$ by a Fierz transformation that is given below. The resulting relative phases are in agreement with the usual symmetry principles. More specifically in this model, the current-current coupling from gluon exchange initiating exchange scattering between valence quarks of two interacting hadrons is taken to effect their spin, color, and flavor exchange. Even when the hadrons are separated, but within a coherence length of the order of m_π^{-1}, it is assumed that this signal (i.e., the t-channel exchange of a color singlet quark-antiquark-gluon system) couples to and thereby propagates through an ordered quark-antiquark condensate chain of the QCD vacuum. Such a nonperturbative process involves a space exchange operator $P(x \leftrightarrow y)$ similar to the permutations that occur in the Bethe Ansatz[14] for condensed matter. In the static limit, the resulting nonlocal quark interchange amplitude therefore takes the form

$$T_Q = -(i\tfrac{2}{3}g)^2 2 \int d^3x\, d^3y\, \bar{\psi}_{c'}(y)(\gamma_\mu 1_f)_{c'd}\psi_d(y) P(x \leftrightarrow y) G(x,y) \bar{\psi}_{d'}(x)(\gamma^\mu 1_f)_{d'c}\psi_c(x) , \tag{1.1}$$

where $\frac{4}{9}$ is the appropriate color matrix element, 1_f denotes the unit matrix in flavor space, and the ψ's are bag wave functions of valence quarks. Through the Fierz transformation

$$2(1_f)_{c'd}(1_f)_{d'c}(\gamma_\mu)_{c'd}(\gamma^\mu)_{d'c} \equiv \sum_\alpha 0^\alpha_{c'c} 0^\alpha_{d'd} , \tag{1.2}$$

T_Q generates precisely those vertex invariants

$$0^\alpha = \left[1, i\gamma_5, \frac{i}{\sqrt{2}}\gamma_\nu, \frac{i}{\sqrt{2}}\gamma_5\gamma_\nu\right](\vec{\tau})^T$$

($T=0$ isoscalar and $T=1$ isovector channel), which occur in the OBE interactions. In our model, this is the origin from which the SU(6) symmetry derives in color dynamics. No adjustable parameters are introduced except those of the underlying bag model which are determined from hadron spectroscopy including the meson masses.

The penetration depths, i.e., self-energy corrections $m_\alpha{}^2$ in the color singlet $(Q\bar{Q})$ condensate propagator G in (1.1), of the exchanged color singlet gluon-$Q\bar{Q}$ system into the quark-antiquark condensate of the QCD vacuum are taken to depend on the symmetry properties of the quark-antiquark component $\bar{\psi}0^\alpha\psi$. Consequently, T_Q may now be written in the form

$$T_Q = \tfrac{4}{9}g^2 \sum_\alpha \left\{ \int d^3x\, \bar{\psi}_{d'}(x) 0^\alpha \psi_d(x) e^{i\vec{q}\cdot\vec{x}} (q^2 - m_\alpha{}^2)^{-1} \int d^3y\, \bar{\psi}_{c'}(y) 0^\alpha \psi_c(y) e^{-i\vec{q}\cdot\vec{y}} \right\} , \tag{1.3}$$

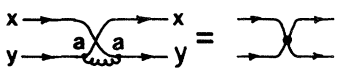

FIG. 1. Nonperturbative, nonlocal quark interchange mechanism.

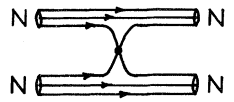

FIG. 2. *NN* OBE via quark interchange.

which exhibits the characteristic structure of OBE interactions. The m_α are taken to be the $(Q\bar{Q})J^\pi T$ (meson) masses, which is consistent with the role of the effective one-gluon exchange in the hadronic (meson) mass formula in bag-model spectroscopy. However, instead of the bag-model meson masses we prefer to use the measured values. Finally, only the valence quarks inside each nucleon are antisymmetrized besides the two nucleons, as if the quarks "knew" to which hadron they belong through color confinement during the collision.

Our purpose here is to study the meson theoretic components of the NN interaction resulting from T_Q in (1.3). We present phase shifts and low energy parameters including the deuteron wave function from the OBE and TBE renormalizations. Our principal aim is not to fit the data but, in a comparison with other more phenomenological, meson theoretic potentials, to isolate their meson exchange contributions from fundamentally different NN force components that may be related to a quark-molecular mechanism at short range.[7]

The paper is organized as follows. In Sec. II we present the OBE formalism and in Sec. III the TBE renormalizations of OBE couplings and form factors. The latter originate from our effective quark interchange in second and third order. The partial-wave helicity-state formalism including the formulas for the axial-vector meson exchanges are given in Sec. IV including a discussion of the methods used to solve the Lippman-Schwinger (LS) equation. Our numerical results are given and discussed in Sec. V.

II. ONE-BOSON EXCHANGE (OBE)

As shown in Ref. 12, the quark interchange amplitude T_Q of (1.3) implies the following OBE representation for the elastic NN amplitude

$$
\begin{aligned}
T_{NN}^{(\mathrm{OBE})}=\tfrac{4}{9}g^2\{\,& F_0^{(-)2}[9(q^2-m_\epsilon{}^2)^{-1}+\vec{\tau}'\cdot\vec{\tau}(q^2-m_\delta{}^2)^{-1}]-g_0{}^2\gamma_5'\gamma_5[(q^2-m_\eta{}^2)^{-1}+\tfrac{25}{9}\vec{\tau}'\cdot\vec{\tau}(q^2-m_\pi{}^2)^{-1}]\\
&-\tfrac{1}{2}[F_{10}\gamma_\mu'+F_{20}i\sigma_{\mu\nu}'q^\nu/2m_N](q^2-m_\omega{}^2)^{-1}[F_{10}\gamma^\mu-F_{20}i\sigma^{\mu\nu}q_\nu/2m_N]\\
&-\tfrac{1}{2}[F_{11}\gamma_\mu'+F_{21}i\sigma_{\mu\nu}'q^\nu/2m_N]\vec{\tau}'\cdot\vec{\tau}(q^2-m_\rho{}^2)^{-1}[F_{11}\gamma^\mu-F_{21}i\sigma^{\mu\nu}q_\nu/2m_N]\\
&-\tfrac{1}{2}[g_{A,0}\gamma_5'\gamma_\mu'+g_{P,0}\gamma_5'q_\mu][(q^2-m_D{}^2)^{-1}+\tfrac{25}{9}\vec{\tau}'\cdot\vec{\tau}(q^2-m_{A_1}{}^2)^{-1}][g_{A,0}\gamma_5\gamma^\mu-g_{P,0}\gamma_5 q^\mu]\}\,.
\end{aligned}
\tag{2.1}
$$

The form factors in (2.1) are defined as matrix elements of the vertex invariants 0^α with valence quark wave functions taken here from the MIT bag model.

The latter are written as

$$
\psi(\vec{r})=\begin{bmatrix} R_0(r) \\ -iR_1(r)\vec{\sigma}\cdot\hat{r}\end{bmatrix}\chi\,, \tag{2.2}
$$

where the radial wave functions $R_{0,1}$ are given in Refs. 6 and 12. With the notation

$$
\begin{aligned}
&F_l(f)=4\pi\int_0^R dr\, r^2 j_l(qr)f(r)\,,\\
&q=|\vec{q}\,|,\ q^2=-\vec{q}^{\,2},\ q=p_1'-p_1=p_2-p_2'\,,
\end{aligned}
\tag{2.3}
$$

the form factors take the following form

$$
\begin{aligned}
&F_0^{(\pm)}=F_0(R_0{}^2\pm R_1{}^2)\,,\\
&g_0=-\frac{4m_N}{q}F_1(R_0\cdot R_1)\,,\\
&F_{1T}=(1-q^2/4m_N{}^2)^{-1}[G_{ET}-(q^2/4m_N{}^2)G_{MT}]\,,\\
&F_{2T}=(1-q^2/4m_N{}^2)^{-1}[G_{MT}-G_{ET}]\,,\\
&G_{ET}=3^{1-T}F_0^{(+)},\ G_{MT}=(\tfrac{5}{3})^T g_0,\ (T=0,1)\,,\\
&g_{A,0}=F_0(R_0{}^2-\tfrac{1}{3}R_1{}^2)+\tfrac{2}{3}F_2(R_1{}^2)\,,\\
&g_{P,0}=-\frac{4m_N}{q^2}F_2(R_1{}^2)\,.
\end{aligned}
\tag{2.4}
$$

For $q\le 0.5$ GeV/c, the momentum transfer dependence of these form factors can be equally well approximated by $[\Lambda^2/(\Lambda^2-q^2)]^n$ with regulator $\Lambda=0.64$ GeV/c for $n=1$ (monopole shape) and $\Lambda=0.9$ GeV/c for $n=2$. The dipole shape is close to the empirical proton charge form factor and is therefore adopted in the following. These shapes

are smooth extrapolations for $q > 0.5$ GeV/c, where the MIT-bag form factors start spurious oscillations that are caused by the underlying infinite square-well potential and do not exist for a linear or harmonic oscillator confinement potential. More accurate monopole and dipole approximations may be obtained (cf. Table I) but the uncertainties (e.g., recoil corrections) of the MIT bag model are larger than the differences between the calculated form factors.

The long range (i.e., monopole regulator $\Lambda = 0.5-0.65$ GeV/c) of our theoretical OBE form factors is a novel feature which contrasts with the larger values and fairly wide interval, $1.2 \lesssim \Lambda \lesssim 2.5$ GeV/c, in phenomenological OBE potentials.[3] In addition to (2.1, 2.4), higher order quark interchanges generate form factor renormalizations with a similar falloff in q, as we shall discuss below.

The values of the coupling constants involving the form factors at $\vec{q}^2 = 0$ are listed in Table II for the effective quark mass parameter $m_Q = 0.108$ GeV/c^2, on which the bag spectroscopy depends. We note that a linear confinement potential[15] yields similar coupling constants that are also listed (for $\alpha_c = 1.9$).

A comparison of our calculated coupling constants with those fitted in more phenomenological OBE models shows several discrepancies. First, our value for the ω-vector coupling, 5—6 in Table II, is consistent with the SU(6) symmetry but provides too little repulsion for the $^1S_0$ and $^3S_1$ phase shifts. Quark interchanges in second and third order corresponding to TBE do not modify the ω-vector coupling significantly. This weakened repulsion at short range is only partially restored by the additional A_1-meson exchange which is increased to ~ 1.4 by higher order renormalization. Comparing our weak ω-vector and A_1 coupling with those of the Paris potential (11.75 and 14, respectively) suggests that these larger fitted values simulate repulsive interactions of nonmesonic origin which may be related to the short range repulsion generated by the quark-molecular mechanism.[7]

Second, our calculated ϵ and δ couplings are fairly weak and short ranged, if the physical masses of these mesons are used in the OBE (2.1). This assumption may be particularly questionable for scalar mesons because of possible appreciable multi-$Q\bar{Q}$ admixtures.[16] These ϵ-δ exchanges together do not provide enough attraction at medium range. In the following section we shall verify that, in second and third order with intermediate nucleon and $\Delta(1232)$ isobar states, the quark interchange T_Q produces low-mass effective scalar-meson exchanges of the correct order of magnitude which correspond to TPE contributions or $(Q\bar{Q})^2$ components of exchanged scalar mesons.

TABLE I. Form factor shapes for $q \leq 1$ GeV/c and $m_Q = 0.108$ GeV/c^2.

Form factor	Λ (GeV/c) monopole ($n=1$)	Λ (GeV/c) dipole ($n=2$)
$F_0(R_0^2 - R_1^2)$	0.615	0.920
$F_0(R_0^2 + R_1^2)$	0.520	0.780
$\frac{4m_N}{q} F_1(R_0 R_1)$	0.605	0.910
$F_0(R_0^2 - \frac{1}{3}R_1^2) + \frac{2}{3}F_2(R_1^2)$	0.610	0.915
$\frac{1}{q^2} F_2(R_1^2)$	0.725	1.075
$F_0(R_0^2 + R_1^2) + \frac{5}{3} \cdot \frac{4m_N}{q} F_1(R_0 R_1)$	0.710	0.910
$F_0(R_0^2 + R_1^2) - \frac{5}{3} \cdot \frac{q}{m_N} F_1(R_0 R_1)$	0.600	0.900
$3F_0(R_0^2 + R_1^2) + \frac{4m_N}{q} F_1(R_0 R_1)$	0.405	0.615
$3F_0(R_0^2 + R_1^2) - \frac{q}{m_N} F_1(R_0 R_1)$	0.510	0.770

TABLE II. OBE interaction parameters.

Meson	Mass (MeV/c^2)	Unrenormalized Refs. 23 and 12	Renormalized	Lin. conf. pot. Refs. 15 and 12	Ref. 19	Bonn[3]
ϵ	1200	3.89	3.89	4.53		
δ	960	0.44	0.47	0.503		6.12
η	548.5	4.87	6.68	5.32	8.05	2
π	138.5	13.4	14.14	14.8	14.4	14
ω	782.3	6 (0.37)	6 (0.37)	3.78(−0.49)	9.05(−0.1)	9.8(0)
ρ	763	0.67(2.16)	0.67(4.2)	0.42(3.18)	0.605(4.78)	0.7(4.5)
D	1285	0.33(1.55)	0.33(1.55)	0.22		
A_1	1100	0.94(1.55)	1.39(1.27)	0.6		
σ_0	495		5.17		6.8	5.04
σ_1	495		0.08			

III. TBE RENORMALIZATIONS

The second order iteration of the quark interchange force T_Q (cf. Fig. 3) with intermediate N,N^* or $\Delta(1232)$ states corresponds to isobar-TBE configurations.[17] If we restrict ourselves to the $\gamma_5\vec{\tau}$ part of T_Q and one intermediate $\Delta(1232)$, then we obtain the TPE amplitude in the static approximation, viz.,

$$T_{\pi\pi}^{(\Delta N)}=-\frac{1}{4m_N{}^4D}\int\frac{d^3q_1}{(2\pi)^3}\frac{g_{\pi N\Delta}(\vec{q}_2)g_{\pi NN}(\vec{q}_2)g_{\pi N\Delta}(\vec{q}_1)g_{\pi NN}(\vec{q}_1)}{(\vec{q}_1{}^2+m_\pi{}^2)(\vec{q}_2{}^2+m_\pi{}^2)}(\vec{S}_1^\dagger\cdot\vec{q}_2\vec{\sigma}_2\cdot\vec{q}_2)\vec{T}_1^\dagger\cdot\vec{\tau}_2\vec{T}_1\cdot\vec{\tau}_2(\vec{S}_1\cdot\vec{q}_1\vec{\sigma}_2\cdot\vec{q}_1)\,, \tag{3.1}$$

where

$$q_1+q_2=q=p_1'-p_1=p_2-p_2'$$

is the overall momentum transfer, and $\vec{S}$, $\vec{T}$ are the spin-isospin $\frac{1}{2}\to\frac{3}{2}$ transition operators of the $\pi N\Delta$ vertex. The form factors are[12]

$$\begin{aligned}
g_{\pi NN}(q)&=-\tfrac{5}{3}(\tfrac{2}{3}g)\left[\frac{4m_N}{q}F_1\right],\\
g_{\pi N\Delta}(q)&=-\sqrt{2}(\tfrac{2}{3}g)\left[\frac{4m_N}{q}F_1\right],\\
f_{\pi N\Delta}&\equiv\frac{m_\pi}{m_N}g_{\pi N\Delta}\,,
\end{aligned} \tag{3.2}$$

TABLE III. Renormalized OBE interaction parameters (strong ρ-tensor).

Meson	Mass (MeV/c^2)	$g^2/4\pi$	f/g
σ_0	495	5.41	
σ_1	495	0.05	
ρ	763	0.67	5.82
D	1285	1.1	0.9

and $D=m_\Delta-m_N$ is the static energy denominator. The following identities

$$\begin{aligned}
&\vec{T}_1^\dagger\cdot\vec{\tau}_2\vec{T}_1\cdot\vec{\tau}_2=2+\tfrac{2}{3}\vec{\tau}_1\cdot\vec{\tau}_2\,,\\
&\vec{T}_1^\dagger\cdot\vec{T}_2^\dagger\vec{T}_1\cdot\vec{T}_2=\tfrac{4}{3}-\tfrac{2}{9}\vec{\tau}_1\cdot\vec{\tau}_2\,,\\
&\vec{S}_1^\dagger\cdot\vec{q}_2\vec{S}_1\cdot\vec{q}_1=\tfrac{2}{3}\vec{q}_2\cdot\vec{q}_1-\frac{i}{3}\vec{\sigma}_1\cdot(\vec{q}_2\times\vec{q}_1)\,,\\
&\vec{\sigma}_2\cdot\vec{q}_2\vec{\sigma}_2\cdot\vec{q}_1=\vec{q}_2\cdot\vec{q}_1+i\vec{\sigma}_2\cdot(\vec{q}_2\times\vec{q}_1)
\end{aligned} \tag{3.3}$$

serve to isolate the spin-independent components in (3.1) which can then be parametrized as effective σ_0

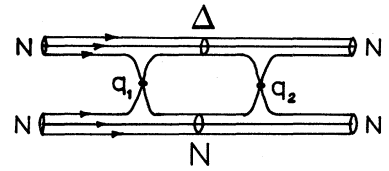

FIG. 3. Iterated quark interchange corresponding to ΔN isobar configuration.

and σ_1 (i.e., $T=0,1$) scalar meson exchanges with monopole form factor shape, viz.,

$$T_{\pi\pi,\sigma_j}=-\frac{g_j^2}{\vec{q}^2+m_j^2}\left[\frac{\Lambda_j^2}{\Lambda_j^2+\vec{q}^2}\right]. \tag{3.4}$$

For $m_Q=0.108$ GeV/c^2 we obtain $m_{0,1}=0.5$ GeV/c^2, $\Lambda_{0,1}=0.725$ GeV/c, $g_0^2/4\pi=0.9$, and $g_1^2/4\pi=0.5$ in $T=1$ NN channels. The $(\Delta\Delta)$ intermediate states are treated similarly, and are found to give the same form of effective σ_0 and σ_1 exchanges but are smaller in strength, viz., 0.52 and 0.30, respectively, in all NN channels. Numerically the effective σ_0 exchange from ΔN, $N\Delta$, and $\Delta\Delta$ isobar configurations provides about 20% of the required attraction at medium range, and it lies in the lowest scalar-meson mass range around 0.5 GeV/c^2. The relatively small contribution from isobar configurations agrees with the results reported in Ref. 3. Crossed TPE diagrams which correspond to higher order quark interchanges and noniterative TPE contributions are not considered here but are known[18] to contribute to the attraction at medium range about equally. Thus our calculations provide only a crude σ_0 estimate.

The spin dependent part of Eqs. (3.1) and (3.3) can be written as effective vector-meson tensor coupling, viz.,

$$T_{\pi\pi}^{(v)}=-(\tfrac{2}{3})^3\frac{(3+\vec{\tau}_1\cdot\vec{\tau}_2)(\vec{\sigma}_1\times\vec{q})\cdot(\vec{\sigma}_2\times\vec{q})}{(4\pi m_\pi m_N)^2(m_\Delta-m_N)}\times\int_0^\infty\frac{dq_1 q_1^4}{\vec{q}_1^2+m_\pi^2}(A_0-\tfrac{1}{5}A_2)g_{\pi NN}(\vec{q}_1)\times f_{\pi N\Delta}(\vec{q}_1)\,,$$
$$A_l=(l+\tfrac{1}{2})\int_{-1}^{1}\frac{dx\,P_l(x)}{\vec{q}_2^2+m_\pi^2}g_{\pi NN}(\vec{q}_2)f_{\pi N\Delta}(\vec{q}_2)\,,\quad \vec{q}_2=\vec{q}_1-\vec{q},\ x=\hat{q}_1\cdot\hat{q}\,. \tag{3.5}$$

In third order, quark interchanges generate various mesonic triangle diagrams. Consequently, double counting with isobar configurations and the OBE is avoided because the latter originate from different quark interchange iterations. Next we estimate the TPE triangle mechanism ($A=N$ or Δ, $\alpha=\beta=\pi$, $\gamma=\sigma_0\equiv\epsilon$ in the TPE mass range, Fig. 4) involving πN S-wave scattering on one nucleon. We take the intermediate nucleon or $\Delta(1232)$ on its mass shell. Occasionally we will also compare to time-ordered perturbation theory which generally yields underestimates. To normalize properly the πN S-wave bag-model amplitude[12] we compare with one from ρ dominance,

$$f_\rho(q+q')_\mu i\epsilon_{\alpha\beta\gamma}\langle N'\,|\,J^\mu\,|\,N\rangle(\vec{q}^{\,2}+m_\rho^2)^{-1}$$

with $f_\rho=\frac{2}{3}g\sqrt{2}$, which yields the normalization constant $2m_\pi$. Thus the isoscalar component of

$$T_{\pi N}=(\tfrac{2}{3}g)^2\bar{u}(p')\left[\frac{6F_0^{(-)2}\delta_{\alpha\beta}2m_\pi}{q^2-m_{\sigma_0}^2}-i\epsilon_{\alpha\beta\gamma}\tau_\gamma F_0^{(+)}(p+p')_\mu(q^2-m_\rho^2)^{-1}(F_{11}\gamma^\mu+iF_{21}\sigma^{\mu\nu}q_\nu/2m_N)\right]u(p) \tag{3.6}$$

is substituted in the triangle amplitudes with an intermediate $\Delta(1232)$. This yields the following isoscalar-scalar TPE contribution

$$T_{\sigma_{0,\Delta}}=(\tfrac{2}{3}g)^4 2m_\pi\cdot\int\frac{d^3q_1}{(2\pi)^3}\left[-\frac{4\sqrt{2}}{q_2}F_1\vec{S}_1^\dagger\cdot\vec{q}_2\right]\vec{T}_1^\dagger\cdot\vec{T}_1\left[-\frac{4\sqrt{2}}{q_1}F_1\vec{S}_1\cdot\vec{q}_1\right]$$
$$\times 6F_0^{(-)2}(q^2)(\vec{q}^2+m_{\sigma_0}^2)^{-1}(\vec{q}_1^{\,2}+m_\pi^2)^{-1}(\vec{q}_2^{\,2}+m_\pi^2)^{-1}\,. \tag{3.7}$$

Using (3.3) to decompose $T_{\sigma_{0,\Delta}}$, the spin independent part of (3.7) can be parametrized as in Eq. (3.4) with the strength

$$\frac{1}{4\pi}g_{\sigma_{0,\Delta}}^2=\frac{4}{3m_\pi}g_{\pi\pi\epsilon}g_{\epsilon NN}\times\int_0^\infty\frac{dq_1 q_1^4}{(2\pi)^3}\frac{f^2_{\pi N\Delta}(q_1)}{\omega_\pi^4(q_1^2)}\,, \tag{3.8}$$

where

$$g_{\pi\pi\epsilon}=\tfrac{2}{3}g\,2F_0^{(-)}\,,\quad g_{\epsilon NN}=\tfrac{2}{3}g\,3F_0^{(-)}\,,\quad \omega_\pi^2(q_1^2)=m_\pi^2+\vec{q}_1^{\,2}\,. \tag{3.9}$$

For $m_Q=0.108$ GeV/c^2 and the dipole shape with $\Lambda=0.9$ GeV/c for the form factors, this contributes

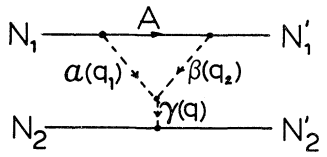

FIG. 4. TBE triangle mechanism.

1.5 to the effective σ_0 strength, with a monopole form factor regulator $\Lambda_0=0.6$ GeV/c.

The corresponding contribution from an intermediate nucleon in Fig. 4 can be written similarly

$$\frac{1}{4\pi}g_{\sigma_{0,N}}{}^2=\frac{3m_\pi}{4m_N{}^2}g_{\pi\pi\epsilon}g_{\epsilon NN}\times\int_0^\infty\frac{dq_1q_1{}^4}{(2\pi)^3}\frac{g_{\pi NN}{}^2(q_1)}{\omega_\pi{}^4(q_1{}^2)}\ , \quad (3.10)$$

and this contributes 1.17 to the σ_0 strength.

In time ordered perturbation theory, $\omega_\pi{}^{-3}$ in Eq. (3.7) is replaced with

$$[(\omega_\pi+m_\Delta-m_N)^{-2}+\omega_\pi{}^{-1}(\omega_\pi+m_\Delta-m_N)^{-1}]/(2\omega_\pi)\ .$$

This expression reduces the radial integral in (3.7) by $\frac{1}{2}$ and is known[17] to give an underestimate, whereas the static approximation (3.7) may overestimate somewhat. Altogether we obtain a σ_0 strength ~ 4.1 from $\Delta N+N\Delta+\Delta\Delta$ isobar configurations and $\pi\pi N+\pi\pi\Delta$ triangle graphs, which supplies the bulk of the known attraction at medium range. We have estimated the contributions from nucleon resonances in the mass range 1.5 to 2 GeV/c^2 and find them capable of providing additional σ_0 strength, but little σ_1 strength. All together our conclusion confirms that the bulk of the attraction at medium range comes from a variety of mesonic TPE mechanisms including crossed diagrams.

The effective $\sigma_{0,1}$ exchanges are particular cases of triangular TBE contributions (third order quark interchanges, cf. Fig. 4) which generally renormalize the OBE coupling constants and form factors. The following estimates are based on the $\pi\pi\epsilon$, $\pi\pi\rho$, $\pi\eta\delta$, and $\pi\rho A_1$ couplings in triangular TBE diagrams.

The πNN vertex renormalization due to the $\pi\pi\epsilon$ triangle mechanisms with an intermediate nucleon state takes the form (with an ϵ mass again in the σ_0 mass range $0.5\lesssim m_\epsilon\lesssim 0.7$ GeV/c^2)

$$T_{\pi,\sigma_0N}=-2m_\pi\frac{g_{\pi NN}^{(\mathrm{OBE})}(\vec{q})}{\vec{q}^2+m_\pi{}^2}(\vec{\tau}_1\cdot\vec{\tau}_2)\frac{\vec{\sigma}_1\cdot\vec{q}}{2m_N}g_{\pi\pi\epsilon}(\vec{q})\times\int\frac{d^3q_1}{(2\pi)^3}\frac{g_{\pi NN}(\vec{q}_1)g_{\epsilon NN}(\vec{q}_2)}{(\vec{q}_1{}^2+m_\pi{}^2)(\vec{q}_2{}^2+m_\epsilon{}^2)}\frac{\vec{\sigma}_2\cdot\vec{q}_1}{2m_N}\ , \quad (3.11)$$

where $\vec{q}_1+\vec{q}_2=\vec{q}$. Since T_{π,σ_0N} can be parametrized as

$$-\frac{g_{\pi NN}^{(\mathrm{OBE})}g_{\pi NN}^{(N)}}{\vec{q}^2+m_\pi{}^2}\vec{\tau}_1\cdot\vec{\tau}_2\frac{\vec{\sigma}_1\cdot\vec{q}\,\vec{\sigma}_2\cdot\vec{q}}{4m_N{}^2}$$

with roughly the same q dependence as the π exchange in (2.1), these triangle graphs define the renormalized coupling

$$g_{\pi NN}=g_{\pi NN}^{(\mathrm{OBE})}+g_{\pi NN}^{(N)}\ ,$$

$$g_{\pi NN}^{(N)}=-\frac{2m_\pi}{3}g_{\pi\pi\epsilon}(\vec{q})\int_0^\infty\frac{dq_1q_1{}^4g_{\pi NN}^{(\mathrm{OBE})}(q_1)}{\pi^2(q_1{}^2+m_\pi{}^2)}\times\frac{d}{d\vec{q}_1{}^2}\left[\frac{g_{\epsilon NN}(\vec{q}_1)}{\vec{q}^{\,2}+\vec{q}_1{}^2+m_\epsilon{}^2}\right]\ . \quad (3.12)$$

The resulting renormalization increases $g_{\pi NN}$ by 12% for $m_Q=0.108$ GeV/c^2 and $m_\epsilon=0.5$ GeV/c^2. The πNN renormalization due to the $\pi\eta\delta$ triangle is much smaller.

However, the ρ meson exchange part of $T_{\pi N}$ in the $\pi\pi\rho$ triangle graphs generates a negative renormalization of $g_{\pi NN}^{(\mathrm{OBE})}$,

$$g_{\pi NN}^{(N,\rho)}=-(\tfrac{5}{3})^2(\tfrac{2}{3}g)^3 2\times\int_0^\infty\frac{dq_1q_1{}^4}{3\pi^2m_N}\cdot\frac{\left[\frac{4m_N}{q_1}F_1\right]^2}{(q_1{}^2+m_\pi{}^2)(q_1{}^2+m_\rho{}^2)}\ , \quad (3.13)$$

which subtracts 24% for $m_Q=0.108$ GeV/c^2. There is a smaller contribution, -8%, from the $\pi\pi\rho$ triangle graphs with an intermediate $\Delta(1232)$ such that $g_{\pi NN}^{(\Delta,\rho)}=8g_{\pi NN}^{(N,\rho)}/25$ at $\vec{q}^{\,2}=0$. Both negative contributions are just about cancelled by the positive $g_{\pi NN}$ renormalization due to the center-of-mass (recoil) form factor correction.[12] All together the πNN renormalizations increase the πNN strength from 13.4 in Table II close to the phenomenological value 14–15 which is therefore used in our numerical calculations.

The $\pi\pi\rho$ triangle TPE mechanisms with an inter-

mediate nucleon and $\Delta(1232)$, $T_{\rho,N}$ and $T_{\rho,\Delta}$, also renormalize the ρ-tensor coupling, while the ρ-vector coupling is hardly affected by the $T_{\pi N}$ component involving $(q_1-q_2)_0\cdot\langle N_1|(\gamma_0\tau_\gamma)|N_1\rangle$. In order to separate the Dirac (γ_μ) and ρ-tensor parts, we write

$$T_{\rho,N}=\tfrac{1}{2}(\tfrac{2}{3}g)^4\langle N_1'|(-\vec{\gamma}\tau_{1\gamma})|N_1\rangle(\vec{q}^{\,2}+m_\rho^{\,2})^{-1}\times\int\frac{d^3q_1}{(2\pi)^3}\frac{(-i\epsilon_{\alpha\beta\gamma})F_0^{(+)}(q)(\vec{q}_1-\vec{q}_2)}{(\vec{q}_1^{\,2}+m_\pi^{\,2})(\vec{q}_2^{\,2}+m_\pi^{\,2})}\times g_{\pi NN}(\vec{q}_2)\frac{\vec{\sigma}_2\cdot\vec{q}_2}{2m_N}\tau_{2\beta}g_{\pi NN}(\vec{q}_1)\frac{\vec{\sigma}_2\cdot\vec{q}_1}{2m_N}\tau_{2\alpha} \tag{3.14}$$

in the same form as the ρ exchange in the OBE (2.1), i.e.,

$$T_{\rho,N}=(\tfrac{1}{2}f_\rho)^2\langle N_1'|(-\vec{\gamma})_1|N_1\rangle\frac{\vec{\tau}_1\cdot\vec{\tau}_2}{\vec{q}^{\,2}+m_\rho^{\,2}}y_N F_1 i\vec{\sigma}_2 x\hat{q}\,, \tag{3.15}$$

where,[12] according to the ρ exchange in (2.1),

$$\langle N_1'|(\vec{\gamma})|N_1\rangle=y_{\rm OBE}iF_1\vec{\sigma}_1 x\hat{q}\,,\qquad y_{\rm OBE}=-\tfrac{10}{3},\quad f_\rho=\tfrac{2}{3}g\sqrt{2}\,. \tag{3.16}$$

From (3.14) and (3.15) we find

$$y_N=(\tfrac{2}{3})^3(\tfrac{10}{3})^2\frac{\alpha_c}{\pi m_N}\times\int_0^\infty\frac{dq_1 q_1^{\,4}F_0^{(+)}(\vec{q}_1)}{(q_1^{\,2}+m_\pi^{\,2})^2}\left[\frac{4m_N}{q_1}F_1\right], \tag{3.17}$$

$$y_\Delta=2^3y_N/5^2\,.$$

Hence, $y_{\rm OBE}$ is renormalized so that $y_r=y_{\rm OBE}+y_N+y_\Delta$. Now we apply (19′) and (20) of Ref. 12. As a result, the renormalization of the ratio of ρ-tensor to ρ-vector coupling becomes

$$\kappa_r=\tfrac{1}{2}(y_N+y_\Delta)\left[\frac{4m_N}{q}F_1\right]\Big/_{q=0}\,. \tag{3.18}$$

For $m_Q=0.108$ GeV/c^2, $y_N=-1.69$, $y_\Delta=-0.54$, and $\kappa_r=2.13$. The renormalized f/g ratio is $\kappa=\kappa_{\rm OBE}+\kappa_r=5.83$, if $\kappa_{\rm OBE}=3.7$, the value of the isovector magnetic moment of the nucleon and ρ dominance are used. This value of κ is close to the values 6.1–6.7 obtained from πN dispersion analysis.[22] The somewhat low bag model value[12]

$$\kappa_{\rm OBE}=-1+\tfrac{1}{2}y_{\rm OBE}\left[\frac{4m_N}{q}F_1\right]_{q=0}=2.18$$

yields $\kappa=4.31$. We have calculated NN phase shifts with both values. Using the three time-ordered triangle diagrams, instead of the on-mass-shell approximation for the intermediate nucleon and $\Delta(1232)$, yields the somewhat smaller values 3.25–4.75 for κ.

For the A_1 renormalization through the $\pi\rho A_1$ triangle TBE, we find only a moderate increase from ~ 1 to less than 2. Hence, just as for the large value of the fitted ω strength, we reach the conclusion here, too, that the large fitted value, 14, for the A_1 strength $g_{A_1NN}^{\,2}/4\pi$ in the Paris potential, which is repulsive in both $^3S_1$ and $^1S_0$ partial waves, is inconsistent with our meson theoretic quark interchange (that is linked to $Q\bar{Q}$ and gluon condensates) and probably simulates some short range repulsion of quark-gluon origin.

The coupling constants of our OBE in (2.1) and soft form factors are similar to Schierholz's potential[19] which uses as much information as possible from other processes to determine its parameters instead of obtaining best fits to the data as in Refs. 2 and 3. The small σ_1-δ coupling, in particular, has motivated us to look into σ_1-δ renormalizations from the $\pi\eta\delta$ triangle TBE mechanism with an intermediate nucleon. However, we obtain only a small positive renormalization for $g_{\sigma_1 NN}$ so that the total σ_1 strength remains small, viz., $\lesssim 0.7$.

Finally, we have also estimated ladder type 3π-exchange contributions with two intermediate ΔN states from quark interchange in third order and found such contributions to be small and attractive. Second order triangle 3π-exchange mechanisms involving two ρ-meson exchanges as well are also small, $\propto q^2$ and, therefore, do not renormalize the ω coupling constant, in contrast with crossed and noniterative π-ρ exchanges.

The loop integrals in the isobar configuration and triangle mechanisms depend sensitively on the dipole OBE form factor shape characterized by its regulator $\Lambda\simeq 0.9$ GeV/c. We consider our success in reproducing the bulk of the medium range attraction and the ρ-tensor renormalization as a confirmation of the basic underlying OBE including its soft form factors which here come from the effective quark interchange amplitude T_Q.

IV. PARTIAL-WAVE HELICITY-STATE EXPANSION

The covariant helicity-state formalism of Erkelenz[3] is now applied to the OBE + TBE poten-

tial in the NN c.m. system upon choosing the kinematics as shown in Fig. 5. This expansion reduces the Lippmann-Schwinger equation (LS equation),

$$t(\vec{p}\,',\vec{p})=V(\vec{p}\,',\vec{p})-m_N\int\frac{d^3k}{(2\pi)^3}\frac{V(\vec{p}\,',\vec{k})t(\vec{k},\vec{p})}{\vec{k}^2-\vec{p}^{\,2}-i0} \tag{4.1}$$

to its radial form. To satisfy elastic unitarity, both t and V are modified by minimal relativity factors, i.e.,

$$\langle p'\,|\,V\,|\,p\rangle=\left[\frac{m_N}{E(\vec{p}\,')}\right]^{1/2},$$

$$\langle\vec{p}\,'\lambda'\,|\,V_{\rm OBE}\,|\,\vec{p}\lambda\rangle\left[\frac{m_N}{E(\vec{p})}\right]^{1/2}. \tag{4.2}$$

The momentum transfer is $k=p_1'-p_1=p_2'$. In the following we extend this treatment to the axial vector coupling

$$V_A=-A^\mu(1)\frac{g_{\mu\nu}}{q^2-{m_A}^2}A^\nu(2),$$

where

$$A^\mu(i)=\bar{u}(p_i',\lambda_i')\left[g_A\gamma_5\gamma^\mu+\frac{f_A}{2m_N}\gamma_5(p_i'-p_i)^\mu\right]\times\vec{\tau}_i u(p_i,\lambda_i)$$

$$\equiv J_A{}^\mu(i)+J_p{}^\mu(i),\quad (i=1,2). \tag{4.3}$$

In the isoscalar channels A^μ represents the axial current of the D meson and $m_A=m_D$, whereas for the isovector case A^μ represents the A_1 meson with $m_A=m_{A_1}$. The other OBE contributions are presented in Ref. 3 to which we refer for conventions and further details involving the helicities λ, the representation of the nucleon spinors u in that basis, and the partial-wave expansion of the potential matrix elements. It is convenient to define the terms

$$V=-J_A(1)J_A(2)/(q^2-{m_A}^2),$$
$$V_{AP}=-[J_A(1)J_p(2)+J_A(2)J_p(1)]/(q^2-{m_A}^2),$$
$$V_{PP}=-J_p(1)J_p(2)/(q^2-{m_A}^2). \tag{4.4}$$

If we substitute the expressions (4.3) for the vertex factors, and the appropriate spinors are used, the following expressions are obtained:

$$V_{AA}=\frac{-{g_A}^2}{q^2-{m_A}^2}\frac{\epsilon'\epsilon}{4{m_N}^2}\left[4\left[\frac{\lambda_1'p'}{\epsilon'}+\frac{\lambda_1 p}{\epsilon}\right]\left[\frac{\lambda_2'p'}{\epsilon'}+\frac{\lambda_2 p}{\epsilon}\right]\langle\lambda_1'\lambda_2'\,|\,\lambda_1\lambda_2\rangle\right.$$
$$\left.-\left[1+4\frac{\lambda_1'\lambda_1 p'p}{\epsilon'\epsilon}\right]\left[1+4\frac{\lambda_2'\lambda_2 p'p}{\epsilon'\epsilon}\right]\langle\lambda_1'\lambda_2'\,|\,\vec{\sigma}_1\cdot\vec{\sigma}_2\,|\,\lambda_1\lambda_2\rangle\right], \tag{4.5}$$

$$V_{AP}=\frac{-g_A f_A}{q^2-{m_A}^2}\frac{\epsilon'\epsilon}{4{m_N}^2}\left[\frac{2(E'-E)}{m_N}\cdot 4\left[\frac{\lambda_1'\lambda_2'p'^2}{\epsilon'^2}-\frac{\lambda_1\lambda_2 p^2}{\epsilon^2}\right]\right.$$
$$+\left[1+\frac{4\lambda_1'\lambda_1 p'p}{\epsilon'\epsilon}\right]\left[\frac{\lambda_2'p'}{\epsilon'}-\frac{\lambda_2 p}{\epsilon}\right]\left[\frac{\lambda_1'p'-\lambda_1 p}{m_N}\right]$$
$$\left.+\left[1+\frac{4\lambda_2'\lambda_2 p'p}{\epsilon'\epsilon}\right]\left[\frac{\lambda_1'p'}{\epsilon'}-\frac{\lambda_1 p}{\epsilon}\right]\left[\frac{\lambda_2'p'-\lambda_2 p}{m_N}\right]\right]\langle\lambda_1'\lambda_2'\,|\,\lambda_1\lambda_2\rangle, \tag{4.6}$$

$$V_{PP}=\frac{-{f_A}^2}{q^2-{m_A}^2}\frac{\epsilon'\epsilon}{4{m_N}^2}\frac{(E'-E)^2+(\vec{p}\,'-\vec{p})^2}{{m_N}^2}4\left[\frac{\lambda_1'p'}{\epsilon'}-\frac{\lambda_1 p}{\epsilon}\right]\left[\frac{\lambda_2'p'}{\epsilon'}-\frac{\lambda_2 p}{\epsilon}\right]\langle\lambda_1'\lambda_2'\,|\,\lambda_1\lambda_2\rangle. \tag{4.7}$$

Here we used the notation

$$E=E(\vec{p}),\quad E'=E(\vec{p}\,'),$$
$$\epsilon=E+m_N,\quad \epsilon'=E'+m_N, \tag{4.8}$$
$$q^2=(E'-E)^2-(\vec{p}\,'-\vec{p})^2 .$$

The helicity matrix elements $\langle\lambda_1'\lambda_2'\,|\,\lambda_1\lambda_2\rangle$ and $\langle\lambda_1'\lambda_2'\,|\,\vec{\sigma}_1\cdot\vec{\sigma}_2\,|\,\lambda_1\lambda_2\rangle$ depend on the scattering angle θ. Now the partial wave decomposition of V_A can be carried out, and the results for

$$\langle\lambda_1'\lambda_2'\,|\,V_A{}^J(p',p)\,|\,\lambda_1\lambda_2\rangle=2\pi\int_{-1}^{1}d\cos\theta d^J_{\lambda_1-\lambda_2,\lambda_1'-\lambda_2'}(\theta)\langle\lambda_1'\lambda_2'p'\,|\,V_A\,|\,\lambda_1\lambda_2 p\rangle \tag{4.9}$$

are given in the Appendix. To solve the uncoupled singlet LS equation, the Kowalski-Noyes method[20] has been used to remove the singularity in (4.1). The asymptotic wave function is expanded in partial waves

$$\phi_k(p)=\sum_l(2l+1)P_l(\hat{k}\cdot\hat{p})a_k^l(p) , \tag{4.10}$$

where

$$a_k^l(p)=(2\pi)^4t_l(k)f_l(k,p)(p^2-k^2-i0)^{-1} , \tag{4.11}$$

and

$$f_l(k,k)=1,\quad t_l(k)=e^{i\delta l}\sin\delta_l/(2\pi^2k) . \tag{4.12}$$

Using this expression in the radial LS equation generates the singularity-free integral equation for

$$f_l(k,p)=\frac{V_l(k,p)}{V_l(p,p}+4\pi\int_0^\infty\frac{dq\,q^2}{q^2-k^2}\left[\frac{V_l(k,q)V_l(p,k)}{V_l(k,k)}-V_l(p,q)\right]f_l(k,q) . \tag{4.13}$$

Solving (4.13) for the $f_l(k,p)$ with the normalization

$$V(p,k)=4\pi\sum_l V_l(p,k)Y_l(\hat{p})\cdot Y_l(\hat{k}) ,$$

the phase shifts are obtained by principal value integrations

$$\tan\delta_l=-2\pi^2V_l(p,p)\left[1+4\pi\mathrm{P}\int_0^\infty\frac{dkk^2}{k^2-p^2}V_l(p,k)f_l(p,k)\right]^{-1} . \tag{4.14}$$

The coupled equations were solved by the R-matrix method in the basis $|JM\lambda_1\lambda_2\rangle$, where the R matrix elements are real. The R-matrix principal-value integral equation is written schematically as

$$R(p',p;E)=V(p',p)-m_N\int_0^\infty\frac{dk\,k^2}{(2\pi)^3}V(p',k)G_0^P(k,E)R(k,p;E) ,$$
$$G_0^P(k;E)=P\frac{m_N{}^2}{E(k)(k^2-p_0{}^2)} , \tag{4.15}$$

where p_0 is the nuclear on-mass-shell momentum in the c.m. system and $E=(p_0{}^2+m_N{}^2)^{1/2}$. Equation (4.15) is solved using the technique of Ref. 21. The on-shell R-matrix elements are then connected to the phase shifts and mixing angles as follows.[3] For spin singlet $S=0$, and the uncoupled spin triplet $S=1$,

$$\tan{}^S\delta^J=-\frac{m_Np}{(4\pi)^2}{}^SR^J ,$$
$$\tan{}^\pm\delta^J=-\frac{m_Np}{2(4\pi)^2}\left\{{}^{12}R^J+{}^{34}R^J\pm\frac{{}^{12}R^J-{}^{34}R^J-4[J(J+1)]^{1/2}{}^{55}R^J}{(2J+1)\cos2\epsilon_J}\right\} , \tag{4.16}$$
$$\tan2\epsilon_J=-2\frac{[J(J+1)]^{1/2}({}^{12}R^J-{}^{34}R^J)+{}^{55}R^J}{{}^{12}R^J-{}^{34}R^J-4[J(J+1)]^{1/2}{}^{55}R^J} .$$

The ${}^{S}R^{J}$ correspond to the six independent helicity states defined as in the Appendix (A2), i.e., ${}^{S}R^{J}$ for $L'=L=J$, and

$$
\begin{aligned}
&{}^{+}R^{J}=\frac{1}{2J+1}\{(J+1)\cdot{}^{12}R^{J}+J\cdot{}^{34}R^{J}-2[J(J+1)]^{1/2}\cdot{}^{56}R^{J}\},\quad L'=J+1=L;\\
&{}^{-}R^{J}=\frac{1}{2J+1}\{J\cdot{}^{12}R^{J}+(J+1)\cdot{}^{34}R^{J}+2[J(J+1)]^{1/2}\cdot{}^{56}R^{J}\},\quad L'=J-1=L;\\
&{}^{+-}R^{J}=-\frac{[J(J+1)]^{1/2}}{2J+1}\left\{{}^{12}R^{J}-{}^{34}R^{J}+\frac{J+1}{[J(J+1)]^{1/2}}\cdot{}^{55}R^{J}-\frac{J}{[J(J+1)]^{1/2}}\cdot{}^{66}R^{J}\right\},\quad L'=J+1,L=J-1;\\
&{}^{-+}R^{J}=-\frac{[J(J+1)]^{1/2}}{2J+1}\left\{{}^{12}R^{J}-{}^{34}R^{J}-\frac{J}{[J(J+1)]^{1/2}}\cdot{}^{55}R^{J}+\frac{J+1}{[J(J+1)]^{1/2}}{}^{66}R^{J}\right\},\quad L'=J-1,L=J+1;
\end{aligned}
\tag{4.17}
$$

which arise in the diagonalization of

$$
\begin{bmatrix} {}^{-}R^{J} & {}^{-+}R^{J} \\ {}^{+-}R^{J} & {}^{+}R^{J} \end{bmatrix}=U^{-1}\begin{bmatrix} R_1 & 0 \\ 0 & R_2 \end{bmatrix}U
$$

with

$$
U=\begin{bmatrix} \cos\epsilon_J & -\sin\epsilon_J \\ \sin\epsilon_J & \cos\epsilon_J \end{bmatrix}.
$$

The bound-state integral equations for the deuteron are free of singularities for positive binding energy $E_B=2m_N-p_0$, where $p_0=m_d$ in the deuteron rest frame. In the helicity basis they take the form

$$
\begin{aligned}
{}^{12}\phi^{J}(p)&=-\frac{m_N}{p^2+m_NB}\int_0^{\infty}\frac{dk\,k^2}{(2\pi)^3}[{}^{12}V^{J}(p,k)\,{}^{12}\phi^{J}(k)+{}^{55}V^{J}(p,k)\,{}^{34}\phi^{J}(k)]\,,\\
{}^{34}\phi^{J}(p)&=-\frac{m_N}{p^2+m_NB}\int_0^{\infty}\frac{dk\,k^2}{(2\pi)^3}[{}^{34}V^{J}(p,k)\,{}^{34}\phi^{J}(k)+{}^{12}\phi^{J}(k)]\,.
\end{aligned}
\tag{4.18}
$$

TABLE IV. Dependence of ${}^{1}S_0$ scattering length, effective range, and phase shift upon varying one coupling constant. $g_s=[({g_{\sigma_0}}^2+{g_{\sigma_1}}^2)/4\pi]^{1/2}$, $g'_D=g_D/\sqrt{4\pi}$, $g'_{A_1}=g_{A_1}/\sqrt{4\pi}$.

Varied parameter	a_s (fm)	r_{0s} (fm)	${}^{1}S_0$ phase shift at $E_{\rm lab}$ (MeV) $E_{\rm lab}=1$	50	100	200	300	400
$g_s=2.355$	−22.4	3.27	59.6°	30.3°	14.2°	−4.0°	−14.7°	−21.8°
$g_s=2.340$	−24.9	3.24	61.5°	30.6°	14.5°	−3.7°	−14.4°	−21.6°
$g'_D=0.78$	−96.6	3.02	75.4°	33.7°	17.1°	−1.2°	−11.9°	−19.1°
$g'_D=0.90$	−44.6	3.11	69.5°	32.4°	16.0°	−2.3°	−12.9°	−20.1°
$g'_D=0.95$	−35.7	3.15	66.8°	31.9°	15.5°	−2.7°	−13.4°	−20.6°
$g'_D=1.00$	−29.5	3.19	64.2°	31.3°	15.0°	−3.2°	−13.9°	−21.1°
$g'_{A_1}=1.28$	−61.8	3.06	72.5°	33.1°	16.6°	−1.7°	−12.4°	−19.6°
$g'_{A_1}=1.38$	−24.8	3.24	61.4°	30.7°	14.5°	−3.7°	−14.3°	−21.5°

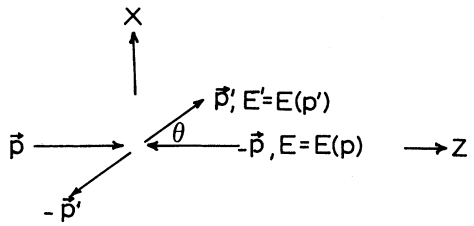

FIG. 5. *NN* kinematics.

The S- and D-state wave functions are linear combinations of ${}^{12}\phi^J$ and ${}^{34}\phi^J$ for $J=1$,

$$\phi_S=\frac{1}{\sqrt{6}}({}^{12}\phi^J+\sqrt{2}{}^{34}\phi^J)\ ,$$
$$\phi_D=\frac{1}{\sqrt{6}}(-\sqrt{2}{}^{12}\phi^J+{}^{34}\phi^J)\ . \tag{4.19}$$

The deuteron D-state probability is calculated from

$$P_D=\int_0^\infty dk\,k^2\phi_D^2/\int_0^\infty dk\,k^2(\phi_S{}^2+\phi_D{}^2)\ , \tag{4.20}$$

and the quadrupole moment from

$$Q_D=\frac{\sqrt{2}}{10}\int_0^\infty dk\left\{k^2\frac{d\phi_S}{dk}\frac{d\phi_D}{dk}+3k\phi_S\frac{d\phi_D}{dk}-\left[k^2\left[\frac{d\phi_D}{dk}\right]^2+6\phi_D{}^2\right]/2\sqrt{2}\right\}. \tag{4.21}$$

The binding energy E_B is found from the homogeneous equations

$$[(1-G_0^P(E)V]\phi=0\ . \tag{4.22}$$

The effective ranges and scattering lengths can also be expressed in the momentum representation.

TABLE V. Dependence of deuteron binding energy E_B and D-state percentage P_D upon varying the triplet σ coupling $g_t=[(g_{\sigma_0}{}^2-3g_{\sigma_1}{}^2)/4\pi]^{1/2}$.

Varied parameter	E_B (MeV)	P_D (%)
$g_t=2.29$	2.170	2.42
$g_t=2.30$	2.337	2.45

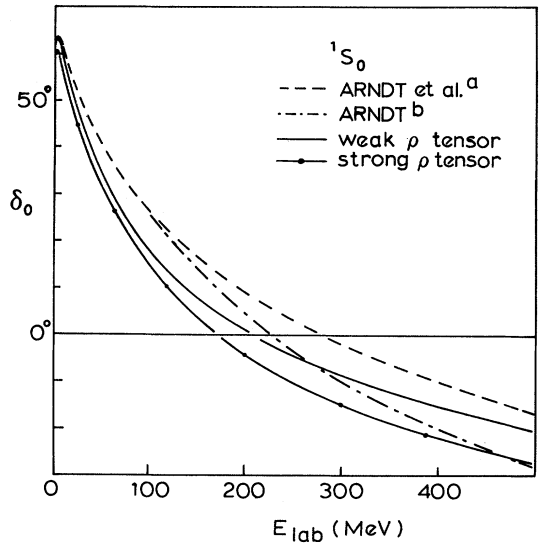

FIG. 6. ${}^1S_0$ phase shift compared with the phase shift analysis of Ref. 25.

In the singlet channel, let us write

$$R(0)={}^0R^0(p'=0,p=0;p_0)$$

for the on-shell R matrix,

$$R(p')={}^0R^0(p',0;p_0)$$

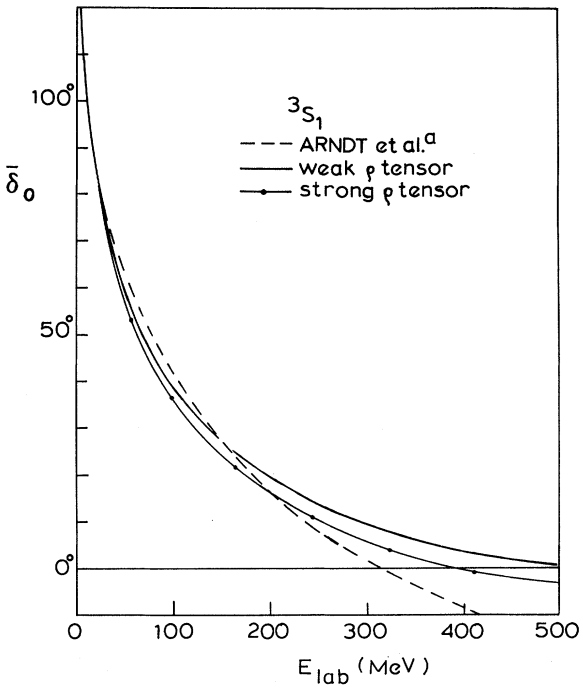

FIG. 7. ${}^3S_1$ Stapp-bar (Ref. 26) phase shift compared with the phase shift analysis of Ref. 25.

TABLE VI. Low energy results for weak and strong ρ tensor coupling.

	Strong ρ tensor	Weak ρ tensor	Experiment
a_s (fm)	−23.4	−23.4	−23.715 ±0.015
r_{0s} (fm)	3.26	2.90	2.73 ±0.03
a_t (fm)	5.66	5.67	5.423 ±0.005
r_{0t} (fm)	2.01	1.97	1.748 ±0.014
E_B (MeV)	2.22	2.217	2.224 62 ±0.000 06
Q_D (fm^2)	0.2486	0.2622	0.2860 ±0.001 5
P_D (%)	2.43	3.1	5 ±3

for the half-on-shell amplitude, and define

$$R''(0)=\lim_{p'\to 0}\frac{1}{p'^2}[R(p')-R(0)] .$$

Then

$$a_s=R(0)/(2\pi) ,$$

$$r_{0s}=\frac{1}{\pi a_s^{\,2}}\left\{R''(0)+\int_0^\infty \frac{dq}{\pi^2 q^2}[R^2(0)-R^2(q)]\right\} , \tag{4.23}$$

$$r_{0t}=\frac{1}{\pi a_t^{\,2}}\left\{R_1''(0)+\int_0^\infty \frac{dq}{\pi^2 q^2}[R_1^2(0)-R_1^2(q)] -2a_t^2\int_0^\infty dp\,\phi_S^{\,2}(p)\right\} ,$$

where R_1 is defined via (4.16) as

$$\tan\delta^J=-\frac{m_N p}{2(4\pi)^2}R_1 .$$

The LS equations were solved numerically. Our computer code was checked for accuracy and reliability by reproducing the results of Erkelenz[3] using his potentials without our A_1 and D meson contributions.

V. RESULTS AND DISCUSSION

The OBE potential (2.1) alone does not fit the NN phase shifts and deuteron properties. At least the effective σ_0 meson exchanges must be included to supply sufficient attraction at medium range. The corresponding results were reported[23] as potential 1.

Here we find that taking into account more systematically the TBE renormalizations of the OBE improves further the agreement with the data.

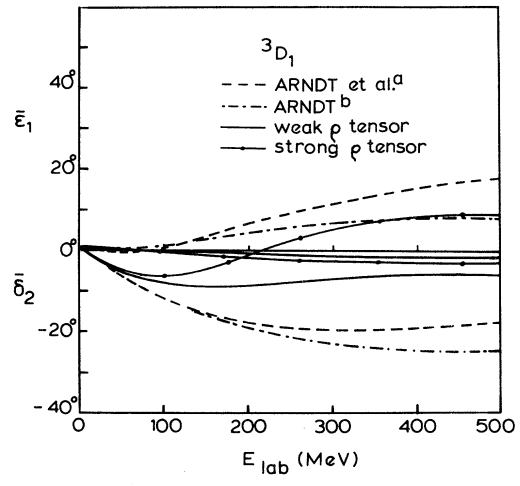

FIG. 8. $^3S_1-{}^3D_1$ Stapp-bar (Ref. 26) phase parameters compared with the phase shift analyses of Ref. 25.

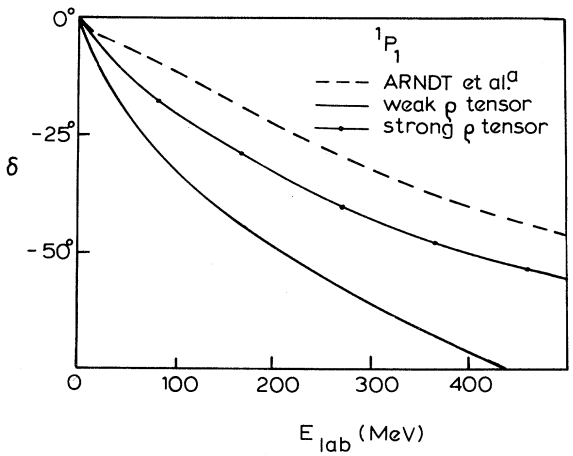

FIG. 9. $^1P_1$ phase shift compared with the phase shift analysis of Ref. 25.

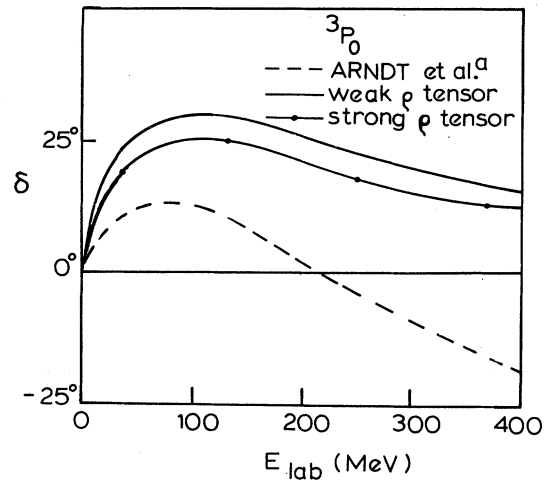

FIG. 10. $^3P_0$ phase shift compared with the phase shift analysis of Ref. 25.

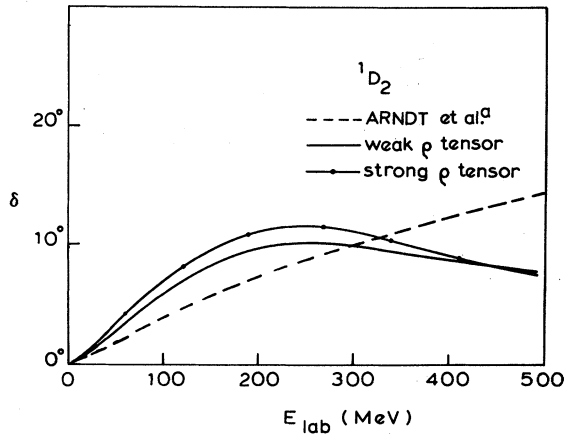

FIG. 12. $^1D_2$ phase shift compared with the phase shift analysis of Ref. 25.

Their effects on the NN interaction can be summarized as

(i) fairly strong σ_0 exchanges (3.4), (3.8), (3.10) from quark interchanges in second order (generating the isobar TPE-box diagram configurations) and quark interchanges in third order (i.e., TPE triangle mechanisms);

(ii) increasing the ρ-tensor strength close to the value, 6, known from πN dispersion relations via third-order quark interchanges (TPE $\pi\pi\rho$ triangles) which improves the $^1P_1$ phase shift significantly; and

(iii) the TBE-triangle renormalizations of the OBE coupling constants from quark interchanges in third order, e.g., πNN, ηNN.

Instead of using the bag model values for the exchanged meson masses (especially for the pion), we prefer here to employ the empirical meson masses. This procedure facilitates also a comparison with other meson theoretic NN potentials. Since the scalar-isoscalar meson is known from the dispersion theoretic treatment of the TPE to have a fairly wide mass distribution, we therefore determine an average σ_0 mass by adjusting the singlet scattering length and the deuteron binding energy. In this process we also determine more precisely the σ_0 and

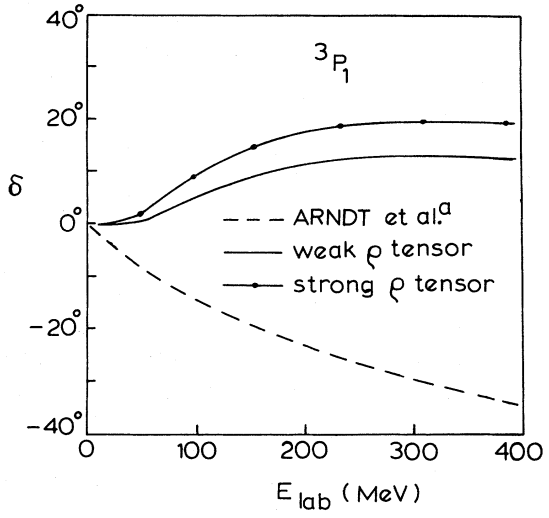

FIG. 11. $^3P_1$ phase shift compared with the phase shift analysis of Ref. 25.

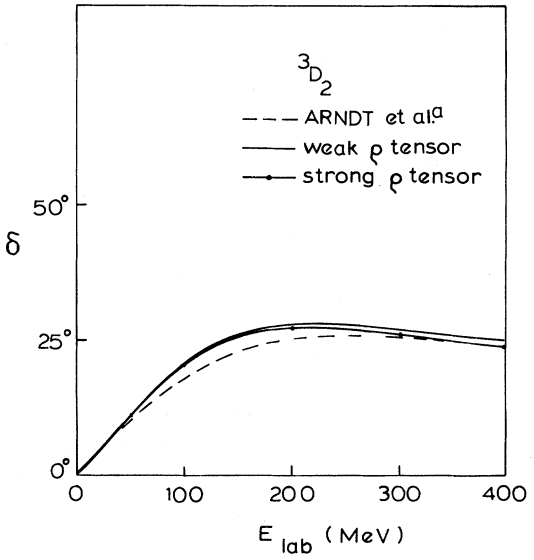

FIG. 13. $^3D_2$ phase shift compared with the phase shift analysis of Ref. 25.

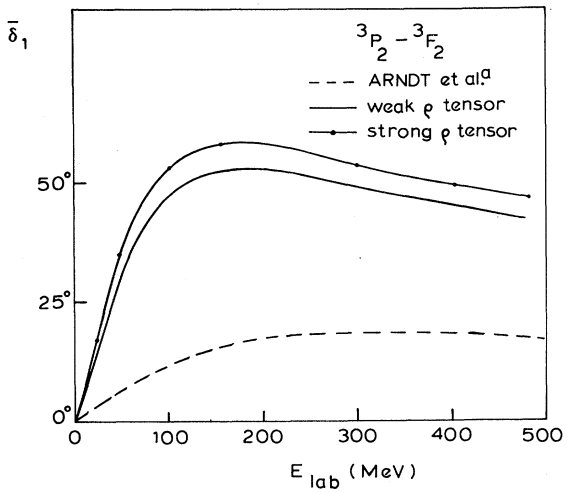

FIG. 14. $^3P_2-^3F_2$ Stapp-bar (Ref. 26) phase parameter compared with the phase shift analysis of Ref. 25.

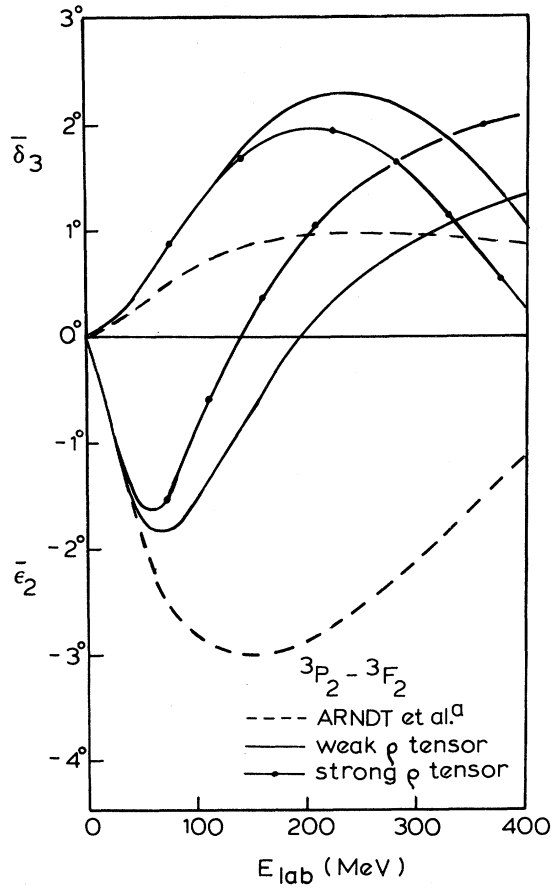

FIG. 15. $^3P_2-^3F_2$ Stapp-bar (Ref. 26) phase parameters compared with the phase shift analysis of Ref. 25.

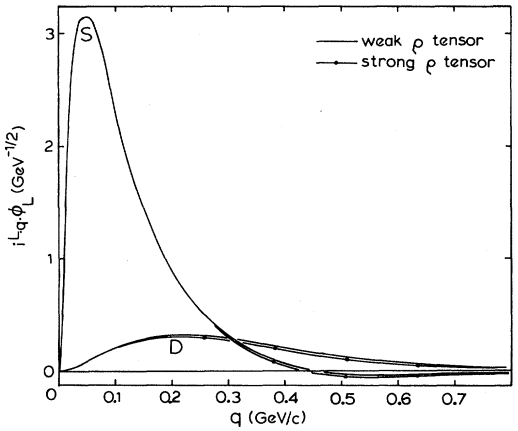

FIG. 16. Deuteron S and D state wave functions.

σ_1 coupling constants which are only crudely estimated in (3.1), (3.4), (3.8), and (3.10). We note in this context that the phase shifts in general, and the scattering lengths and effective ranges particularly, are fairly sensitive to small changes in the σ_0, D, A_1 couplings. In the $^1S_0$ channel, these effects are displayed in Tables IV and V. This way we obtain a reasonable σ_0 mass value $m_{\sigma_0}=0.5$ GeV/c^2, and we take $m_{\sigma_1}=m_{\sigma_0}$. With these interaction parameters, given in Table II for weak ρ-tensor coupling, we are able to reproduce the trend of most of the phase shifts which are displayed in Figs. 6—15 and the remaining low energy parameters that are given in Table VI. For strong ρ-tensor coupling we leave the $\sigma_{0,1}$ couplings almost unchanged but adjust the D-meson coupling somewhat as given in Table III. The D-meson exchange acts attractively in the $^3S_1$ and repulsively in the $^1S_0$ partial waves.

Several of the calculated phase shifts are sensitive to the ρ-tensor coupling. In particular the $^1P_1$ phase shift (see Fig. 9) improves with the strong ρ-tensor value ~ 6. However, upon inspecting all the phase shift results, the preference for the strong ρ-tensor coupling becomes less clear.

We notice that, in general between 0.2 and 0.3 GeV, the calculated phase shifts start to deviate systematically from the data, and some fit the data only qualitatively even below 0.2 GeV. We attribute this feature to insufficient strength, and the lack of repulsion at short range more specifically, in our OBE + TBE potential which contrasts with the more phenomenological NN potentials that contain large, fitted (but theoretically unjustified) values for the ω and, sometimes also for the A_1 meson coupling. Since our quark interchange model appears

to reproduce all meson exchange interactions at low q, this suggests that such an additional NN force has a nonmesonic origin.[7,24]

VI. CONCLUSION

The nonlocal quark interchange amplitude T_Q generates an effective OBE potential with the following characteristic features.

(i) the ω meson has the (low) SU(6) coupling that is not appreciably renormalized in higher orders;

(ii) the momentum-space form factors are soft: they have the dipole shape of the proton charge form factor. This prediction is successfully tested in the calculation of TBE renormalizations which turn out to be correct both in sign and magnitude, and in the calculation of isobar contributions that are reproduced by T_Q in second order. Both involve loop integrals over OBE form factors;

(iii) both the σ_0 and the ρ-tensor coupling are correctly reproduced from TBE renormalizations that use T_Q in second and third order and agree with dispersion relation approaches.

There are some marked differences between our potential and older interactions:

(a) Our results indicate that an expansion of the baryon-baryon interaction in the form OBE + TBE + $\cdots$ should be preferred to the too narrow concept of OPE + TPE + $\cdots$ underlying the dispersion theory of nuclear forces.

(b) The overly large A_1 and ω couplings give phenomenological repulsion in the Paris and the Bonn potentials that, we believe, simulates the effect of short-range repulsion from nonmesonic origin, possibly due to quark-molecular mechanisms.

(c) Our Ansatz for T_Q contains the invariant $\sum_a(\lambda_a'\lambda^a\gamma_\mu'\gamma^\mu)_{\text{exch}}$ in contrast to the color invariant $\sum_a(\lambda_a'\lambda^a)_{\text{dir}}$ of the effective quark potentials.

Finally, we emphasize the main point of this study: Our full renormalized OBE nuclear amplitude is a concrete step towards a calculated NN interaction. It reproduces most phase shifts qualitatively and some even quantitatively.

ACKNOWLEDGMENTS

We thank J. C. H. van Doremalen for helping us with the numerical work which was performed at and supported by the Computer Science Center of the University of Virginia. This work was supported in part by the National Science Foundation.

APPENDIX

Using the expressions given in Ref. 3, we can perform the partial wave analysis. With Erkelenz's notation for

$$V_1^J=\langle++|V^J|++\rangle,\quad V_3^J=\langle+-|V^J|+-\rangle,$$
$$V_2^J=\langle++|V^J|--\rangle,\quad V_4^J=\langle+-|V^J|-+\rangle, \tag{A1}$$
$$V_5^J=\langle++|V^J|+-\rangle,\quad V_6^J=\langle+-|V^J|++\rangle,$$

and the combinations

$$^0V^J=V_1^J-V_2^J,\quad ^1V^J=V_3^J-V_4^J,$$
$$^{12}V^J=V_1^J+V_2^J,\quad ^{34}V^J=V_3^J+V_4^J, \tag{A2}$$
$$^{55}V^J=2V_5^J,\quad ^{66}V^J=2V_6^J,$$

we find

$$^0V_{AA}^J=\frac{2\pi g_A{}^2}{m_N{}^2}\frac{2E'E+m_N{}^2}{p'p}Q_J(Z_A), \tag{A3a}$$

$$^1V_{AA}^J=\frac{-2\pi g_A{}^2}{m_N{}^2}\left[\frac{E'E}{p'p}Q_J(Z_A)+Q_J^{(2)}(Z_A)\right], \tag{A3b}$$

$$^{12}V_{AA}^J=\frac{2\pi g_A{}^2}{m_N{}^2}\left[2Q_J(Z_A)-\frac{m_N{}^2}{p'p}Q_J^{(1)}(Z_A)\right], \tag{A3c}$$

$$^{34}V^J_{AA}=\frac{-2\pi {g_A}^2}{{m_N}^2}\left[Q_J(Z_A)+\frac{E'E}{p'p}Q^{(2)}_J(Z_A)\right], \tag{A3d}$$

$$^{55}V^J_{AA}=\frac{4\pi {g_A}^2}{{m_N}^2}\frac{Em_N}{p'p}Q^{(3)}_J(Z_A), \tag{A3e}$$

$$^{66}V^J_{AA}=\frac{4\pi {g_A}^2}{{m_N}^2}\frac{E'm_N}{p'p}Q^{(3)}_J(Z_A), \tag{A3f}$$

$$^{0}V^J_{AP}=\frac{4\pi g_A f_A}{{m_N}^2}[YQ_J(Z_A)-Q^{(1)}_J(Z_A)], \tag{A4a}$$

$$^{1}V^J_{AP}=\frac{-4\pi g_A f_A}{{m_N}^2}[YQ_J(Z_A)-Q^{(2)}_J(Z_A)], \tag{A4b}$$

$$^{12}V^J_{AP}=\frac{-4\pi g_A f_A}{{m_N}^2}[Q_J(Z_A)-YQ^{(1)}_J(Z_A)], \tag{A4c}$$

$$^{34}V^J_{AP}=\frac{4\pi g_A f_A}{{m_N}^2}[Q_J(Z_A)-YQ^{(2)}_J(Z_A)], \tag{A4d}$$

$$^{55}V^J_{AP}=\frac{-8\pi g_A f_A}{{m_N}^2}\frac{(E'-E)E'E}{m_N p'p}Q^{(3)}_J(Z_A), \tag{A4e}$$

$$^{66}V^J_{AP}=-{}^{55}V^J_{AP}, \tag{A4f}$$

$$^{0}V^J_{PP}=\frac{2\pi {f_A}^2}{{m_N}^4}[(E'E-{m_N}^2)YQ_J(Z_A)-(p'pY-\tfrac{1}{2}{m_A}^2)Q^{(1)}_J(Z_A)-\frac{p'p}{3}\delta_{J1}], \tag{A5a}$$

$$^{1}V^J_{PP}=\frac{-2\pi {f_A}^2}{{m_N}^4}\{(E'E-{m_N}^2)YQ_J(Z_A)-(E'E-{m_N}^2)Q^{(1)}_J(Z_A)-[(E'-E)^2-\tfrac{1}{2}{m_A}^2]Q^{(2)}_J(Z_A)-\tfrac{2}{3}p'p\delta_{J1}\}, \tag{A5b}$$

$$^{12}V^J_{PP}=\frac{-2\pi {f_A}^2}{{m_N}^2}\left\{(p'p)YQ_J(Z_A)-\tfrac{1}{3}(E'E-{m_N}^2)\delta_{J1}-\frac{(E'E-{m_N}^2)[(E'-E)^2-\tfrac{1}{2}{m_A}^2]+{p'}^2p^2}{p'p}Q^{(1)}_J(Z_A)\right\}, \tag{A5c}$$

$$^{34}V^J_{PP}=\frac{2\pi {f_A}^2}{{m_N}^4}\left\{p'pYQ_J(Z_A)-p'pQ^{(1)}_J(Z_A)-\tfrac{2}{3}(E'E-{m_N}^2)\delta_{J1}-\frac{[(E'-E)^2-\tfrac{1}{2}{m_A}^2](E'E-{m_N}^2)}{p'p}Q^{(2)}_J(Z_A)\right\}, \tag{A5d}$$

$$^{55}V^J_{PP}=\frac{4\pi {f_A}^2}{{m_N}^2}\frac{E'-E}{m_N}\left[\frac{(E'-E)^2-{m_A}^2/2}{p'p}Q^{(3)}_J-\frac{\sqrt{2}}{6}\delta_{J1}\right], \tag{A5e}$$

$$^{66}V^J_{PP}=-{}^{55}V^J_{PP}. \tag{A5f}$$

The function $Q_J(Z)$ is Legendre's functions of the second kind; the other Q functions are related to it:

$$\begin{aligned} Q^{(1)}_J(Z)&=Q_J(Z)-\delta_{J0}, \\ Q^{(2)}_J(Z)&=\frac{JZQ_J(Z)+Q_{J-1}(Z)}{J+1}, \\ Q^{(3)}_J(Z)&=\tfrac{1}{2}\left[\frac{J}{J+1}\right]^{1/2}[ZQ_J(Z)-Q_{J-1}(Z)]. \end{aligned} \tag{A6}$$

Furthermore,

$$Z_A=\frac{E'E-m_N{}^2+\frac{1}{2}m_A{}^2}{p'p}\,,$$
$$Y=\frac{E'^2+E^2-E'E-m_N{}^2}{p'p}\,. \tag{A7}$$

[1]See, e.g., *Nucleon-Nucleon Interactions—1977 (Vancouver),* Proceedings of the Second International Conference on Nucleon-Nucleon Interactions, edited by D. Measday, H. Fearing, and A. Strathdee (AIP, New York, 1977).

[2]M. Lacombe, B. Loiseau, J. M. Richard, R. Vinh Mau, J. Coté, P. Pirès, and R. de Tourreil, Phys. Rev. C 21, 861 (1980), and references therein.

[3]K. Erkelenz, Phys. Rep. C13, 191 (1974); K. Holinde, *ibid.* C68, 121 (1981).

[4]See, e.g., *Quantum Chromodynamics,* edited by W. Frazer and F. Henyey (AIP, New York, 1979).

[5]D. J. Gross and F. A. Wilczek, Phys. Rev. Lett. 30, 1343 (1973); H. D. Politzer, *ibid.* 30, 1346 (1973); G. 't Hooft (unpublished).

[6]T. DeGrand, R. Jaffe, K. Johnson, J. Kiskis, Phys. Rev. D 12, 2060 (1975).

[7]D. Liberman, Phys. Rev. D 16, 1542 (1977); C. DeTar, *ibid.*, 17, 323 (1978); 19, 1028 (1979) E; C. S. Warke and R. Shanker, Phys. Rev. C 21, 2643 (1980); M. Harvey, Nucl. Phys. A352, 326 (1981).

[8]O. W. Greenberg and H. J. Lipkin, Fermilab-Report-81/45-THY, 1981.

[9]J. Ambjorn and P. Olesen, Nucl. Phys. B170, 60 (1980); B170, 265 (1980); M. A. Shifman, A. I. Vainstein, V. I. Zakharov, *ibid.* B147, 385 (1979); B147, 448 (1979); B147, 519 (1979); R. Fukuda, Phys. Lett. 73B, 33 (1978).

[10]J. Finger, D. Horn, and J. Mandula, Phys. Rev. D 20, 3252 (1979).

[11]H. Leutwyler, Phys. Lett. 98B, 447 (1981).

[12]H. J. Weber, Z. Phys. A 297, 261 (1980); A 301, 141 (1981); and in *Proceedings of the NATO Advanced Summer Institute, Lahnstein,* edited by W. Greiner (Plenum, New York, 1981).

[13]H. J. Weber and J. N. Maslow, Z. Phys. A 297, 271 (1980).

[14]H. B. Thacker, Rev. Mod. Phys. 53, 253 (1981).

[15]C. L. Critchfield, Phys. Rev. D 12, 923 (1975).

[16]P. Estabrooks, Phys. Rev. D 19, 2678 (1979); A. Bramon and E. Masso, Phys. Lett. 93B, 65 (1980).

[17]H. J. Weber and H. Arenhövel, Phys. Rep. 36C, 277 (1978).

[18]J. W. Durso, M. Saarela, G. E. Brown, and A. D. Jackson, Nucl. Phys. A278, 445 (1977); X. Bagnoud, K. Holinde, and R. Machleidt, Phys. Rev. C 24, 1143 (1981); K. Holinde, R. Machleidt, A. Faessler, H. Müther, and M. R. Anastasio, *ibid.* 24, 1159 (1981).

[19]G. Schierholz, Nucl. Phys. B40, 335 (1972).

[20]K. J. Kowalski and D. Feldman, J. Math. Phys. 4, 507 (1963).

[21]M. Haftel and F. Tabakin, Nucl. Phys. A158, 1 (1970).

[22]G. Höhler and E. Pietarinen, Nucl. Phys. B95, 210 (1975).

[23]B. L. G. Bakker, J. N. Maslow, and H. J. Weber, Phys. Lett. 104B, (1981) 349.

[24]Yu. A. Simonov, ITEP-63, 1981.

[25]R. Arndt, R. H. Hackman, and L. D. Roper, Phys. Rev. C 15, 1002 (1977) (this is analysis a) and R. Arndt in Ref. 1 , p. 117 (this is analysis b).

[26]H. P. Stapp, Phys. Rev. 105, 302 (1957).